Saturation of the Hosing Instability in Quasilinear Plasma Accelerators

R. Lehe,* C. B. Schroeder, J.-L. Vay, E. Esarey, and W. P. Leemans
Lawrence Berkeley National Laboratory, Berkeley, California 94720, USA
(Received 24 June 2017; published 13 December 2017)

The beam hosing instability is analyzed theoretically for a witness beam in the quasilinear regime of plasma accelerators. In this regime, the hosing instability saturates, even for a monoenergetic bunch, at a level much less than standard scalings predict. Analytic expressions are derived for the saturation distance and amplitude and are in agreement with numerical results. Saturation is due to the natural head-to-tail variations in the focusing force, including the self-consistent transverse beam loading.

DOI: 10.1103/PhysRevLett.119.244801

The beam hosing instability is a major concern for both conventional accelerators and plasma-based accelerators. In both cases, this instability can exponentially amplify the small misalignments between the beam and the accelerating structure, and potentially lead to a strong degradation of the beam emittance, or even to complete disruption of the beam. Thus the hosing instability (which is related to the well-known beam-breakup instability) has been actively studied in its various regimes [1]. This includes the long-bunch, weakly coupled regime [2,3] applicable to low-current bunches in conventional accelerators, as well as the long-bunch [4–6] and short-bunch [7–12] strongly coupled regimes, which are of interest for beams propagating in plasmas or ion channels.

In particular, the short-bunch, strongly coupled regime is relevant to the evolution of the witness beam in plasma-wakefield acceleration (both for the beam-driven and laser-driven scheme). In this case, the exponential growth of the hosing instability as a function of the acceleration distance has raised concerns regarding the feasibility of a plasma-based particle collider [13]. However, these predictions have been made in the context of the blowout (or bubble) wakefield regime, i.e., when the driver (beam or laser) is strong enough to expel all the plasma electrons, forming a comoving ion cavity [14–18]. Plasma accelerators may also operate in the quasilinear regime, where the driver excites a plasma density perturbation that is a fraction of the background plasma density [19]. In this Letter, we show that the sustained exponential growth of the hosing instability, which indeed applies for monoenergetic beams in the blowout regime, does not occur in the quasilinear regime. Instead, in the quasilinear regime, the instability can rapidly saturate, and leads only to a moderate amplification of the beam misalignment.

This early saturation is due to the head-to-tail spread in betatron frequency that naturally occurs across the bunch in the quasilinear regime. It is indeed well known that a head-to-tail spread in betatron frequency can mitigate the hosing instability [1,20]. However, in the blowout regime, the focusing force of the wakefield is independent of the longitudinal coordinate, and thus any head-to-tail spread in betatron frequency necessarily requires an energy spread in the bunch. Owing to the typically large beam loading for high efficiency, large energy spreads (e.g., a few percent [11]) are required [13]. This is impractical, since many applications of plasma-wakefield accelerators require monoenergetic beams. By contrast, in the quasilinear regime, the focusing force naturally varies as a function of the longitudinal coordinate, and moreover this variation can potentially be tailored by beam loading [21]. Therefore, in the quasilinear regime, no energy spread is required in order to mitigate the hosing instability.

Hosing equation.—In order to study the hosing instability, let us consider the equation of evolution for the centroid of the witness beam. For simplicity, the effects of beam acceleration are not considered here, but can be obtained by a simple change of variable [10,22] [i.e., by replacing, in Eq. (1) below, x_c by $\tilde{x}_c = [\gamma(z)/\gamma(0)]^{1/4} x_c$ and z by $\tilde{z} = \int_0^z [\gamma(0)/\gamma(z')]^{1/2} dz'$]. Under these assumptions, the transverse evolution of the centroid $x_c(\xi, z)$ is governed by the equation

$$\partial_z^2 x_c(\xi,z) + k_\beta^2(\xi) x_c(\xi,z) = k_c^2 \int_\xi^0 \frac{n_b(\xi')}{n_p} x_c(\xi',z) \sin[\kappa_p(\xi'-\xi)]\kappa_p d\xi', \quad (1)$$

where z is the propagation distance, $\xi = z - ct$ is the head-to-tail coordinate (by convention here, $\xi = 0$ corresponds to the head of the witness bunch, and thus this bunch extends in the region $\xi < 0$), $n_b(\xi)$ is the bunch density at position ξ, and n_p is the plasma density. Physically, the left-hand side of Eq. (1) is the equation of motion in a purely cylindrically symmetric wakefield, while the right-hand side captures the asymmetric perturbations to the wakefield, which are driven by the transverse offset x_c of the beam (see, e.g., Refs. [6,12]). The expression of the coefficients $k_\beta(\xi)$, k_c, and κ_p depend on the wakefield regime considered.

For instance, in the blowout regime [12], Eq. (1) applies with $k_\beta^2(\xi) = k_p^2/2\gamma$, $k_c^2 = (n_p/n_{b,0})k_p^2/2\gamma$, and $\kappa_p = \sqrt{n_{b,0}r_b^2/n_p r_0^2}(c_\psi k_p/\sqrt{2})$ (assuming a uniform bunch density $n_b(\xi) = n_{b,0}$), where k_p is the plasma wave vector, r_b and γ are the radius and Lorentz factor of the monoenergetic witness beam, r_0 is the radius of the blown-out cavity, and the coefficient c_ψ (given in Ref. [12]) takes into account the relativistic nature of the electron sheath. In this regime and for a monoenergetic bunch, there are no head-to-tail variations of the betatron frequency; i.e., k_β is independent of ξ.

On the other hand, in the quasilinear regime (and for a witness beam having a transverse flattop profile with $k_p r_b \ll 1$), Eq. (1) applies with $\kappa_p = k_p$, $k_c^2 = k_p^2/2\gamma$, and

$$k_\beta^2(\xi) = \frac{k_p^2}{2\gamma}\eta_{d\perp}\sin[k_p(\xi_d - \xi)] + \frac{k_p^2}{2\gamma}\int_\xi^0 \frac{n_b(\xi')}{n_p}\sin[k_p(\xi' - \xi)]k_p d\xi', \quad (2)$$

where the first term corresponds to the transverse wakefield generated by the driver (either a laser or a charged particle bunch) and the second term corresponds to transverse beam loading by the witness beam [21]. In the above expression, ξ_d is the average longitudinal position of the driver and $\eta_{d\perp}$ is the amplitude of the transverse driver wakefield. For example, in the case of a flattop electron bunch driver with a density n_d, radius r_d, and length ℓ_d, this amplitude is $\eta_{d\perp} = (n_d/n_p)k_p r_d K_1(k_p r_d)2\sin(k_p\ell_d/2)$, where K_1 is the modified Bessel function. In case of a linearly polarized Gaussian laser pulse with an amplitude $a_0 \lesssim 1$, a waist $w_0 \gg r_b$, and a rms duration τ, $\eta_{d\perp} = \sqrt{8\pi}/(k_p w_0)^2 \times a_0^2(\omega_p\tau)e^{-(\omega_p\tau)^2/2}$. From Eq. (2), it is clear that $k_\beta(\xi)$ exhibits head-to-tail variations, even for a monoenergetic beam. As shown below, these variations can lead to a saturation of the hosing instability.

Analytical solution for a linear chirp.—In the general case, the system Eqs. (1) and (2) can only be solved numerically. However, in order to gain insight into the saturation mechanism, we first study Eq. (1) analytically, in the simplified case of a linear betatron head-to-tail chirp and uniform beam density:

$$k_\beta(\xi) = k_{\beta,0} + (\partial_\xi k_\beta)\xi, \qquad n_b(\xi) = n_{b,0}, \quad (3)$$

where $\partial_\xi k_\beta$ is constant and quantifies the betatron chirp. Note that, although we will eventually apply this analytical solution to the case of a quasilinear wakefield, we keep the generic notations k_c and κ_p from Eq. (1) here, so that the analysis can be applied to other similar situations (e.g., blowout regime with linear energy chirp).

For small betatron chirps ($|(\partial_\xi k_\beta)\xi| \ll k_{\beta,0}$), we find that standard Laplace transform and steepest descents techniques can be applied to find $x_c(\xi, z)$. Starting, for instance, from a uniform initial offset $x_c(\xi, z = 0) = \delta x$, asymptotic solutions can be found for the early stage and late stage of the hosing instability, where the transition between these two asymptotic solutions is determined by a characteristic length,

$$L_{\rm sat}(\xi) = \left(\frac{n_{b,0}}{n_p}\frac{k_c^2\kappa_p^2}{k_{\beta,0}|\partial_\xi k_\beta|^3|\xi|}\right)^{1/2}. \quad (4)$$

(See the Supplemental Material for a derivation of these solutions [23].) For $z \ll L_{\rm sat}(\xi)$ (early stage), the asymptotic solution is given by

$$x_c(\xi, z) = \delta x\frac{\cos[k_\beta(\xi)z - \frac{3}{4}N(\xi,z) + \frac{\pi}{12}]}{(6\pi)^{1/2}N(\xi,z)^{1/2}}e^{(3\sqrt{3}/4)N(\xi,z)},$$
$$\text{with} \quad N(\xi, z) = \left(\frac{n_{b,0}}{n_p}\frac{k_c^2\kappa_p^2 z|\xi|^2}{k_{\beta,0}}\right)^{1/3}, \quad (5)$$

and corresponds to the well-known scaling of the hosing instability, whereby the amplitude of the betatron oscillations grows exponentially with z.

On the other hand, for $z \gg L_{\rm sat}(\xi)$ (late stage), the form of the solution depends on the sign of $\partial_\xi k_\beta$. For $\partial_\xi k_\beta > 0$ (increasing betatron frequency from tail to head), the solution is given by

$$x_c(\xi, z) = \delta x\frac{\cos[k_\beta(\xi)z - \varphi(z)]}{(8\pi^2)^{1/4}N_{\rm sat}(\xi)^{1/2}}e^{\sqrt{2}N_{\rm sat}(\xi)},$$
$$\text{with} \quad N_{\rm sat}(\xi) = N(\xi, L_{\rm sat}) = \left(\frac{n_{b,0}}{n_p}\frac{k_c^2\kappa_p^2|\xi|}{k_{\beta,0}\partial_\xi k_\beta}\right)^{1/2},$$
$$\varphi(z) = \frac{n_{b,0}}{n_p}\frac{k_c^2\kappa_p^2}{2(\partial_\xi k_\beta)^2 k_{\beta,0}z}, \quad (6)$$

and corresponds to betatron oscillations that have a constant, saturated amplitude. For $\partial_\xi k_\beta < 0$ (decreasing frequency from tail to head), the solution is given by

$$x_c(\xi, z) = -\delta x\frac{\sin[k_{\beta,0}z - \varphi(z)]}{(32\pi^2)^{1/4}N_{\rm sat}(\xi)^{-1/2}}\frac{e^{\sqrt{2}N_{\rm sat}(\xi)}}{|\partial_\xi k_\beta z\xi|} + \delta x\frac{\cos[k_\beta(\xi)z - \varphi(z)]}{(\pi^2/2)^{1/4}N_{\rm sat}(\xi)^{1/2}}\cos\left(\sqrt{2}N_{\rm sat}(\xi) - \frac{\pi}{4}\right) \quad (7)$$

and corresponds to betatron oscillations that initially decrease as $1/z$ [first term in Eq. (7)] and eventually saturate at a low level [second term in Eq. (7)].

We note that Refs. [22,24] considered beam breakup in conventional accelerators, and that similar analytical solutions were found in the case of a wakefield function that is

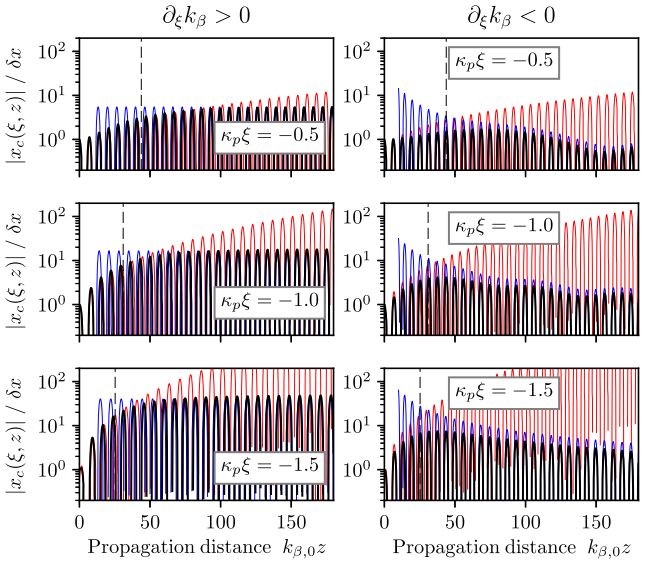

FIG. 1. Comparison of the numerical integration of the hosing equation Eq. (1) in the case of a linear chirp (black curve) with the early-stage solution [Eq. (5); red curve] and the late-stage solution [Eqs. (6) and (7) on the left- and right-hand panels, respectively; blue curve], at different slices along the witness bunch (i.e., different values of $\kappa_p\xi$). The vertical dashed line corresponds to $z = L_{\rm sat}(\xi)$, from Eq. (4). The parameters used here are $k_c^2 n_{b,0}/n_p = k_{\beta,0}^2$ and $\partial_\xi k_\beta = 0.1 k_{\beta,0}\kappa_p$ (left-hand panels) or $\partial_\xi k_\beta = -0.1 k_{\beta,0}\kappa_p$ (right-hand panels).

linear in ξ [i.e., where the sin function in Eq. (1) is replaced by a linear function]. However, this short-beam linear wakefield function does not properly describe plasma accelerators where, typically, $k_p\xi \sim 1$.

The asymptotic solutions Eqs. (5)–(7) are compared with the explicit numerical integration of the hosing equation Eq. (1) in Fig. 1, for $\partial_\xi k_\beta > 0$ (left-hand panels) and $\partial_\xi k_\beta < 0$ (right-hand panels). As expected, in both cases the numerical solution (black curve) is initially in agreement with the standard scaling Eq. (5) (red curve). For longer propagation distances, the instability saturates and is in good agreement with Eqs. (6) and (7), respectively (blue curves). Additionally, Eq. (4) correctly predicts the approximate position of the transition between the early-stage and late-stage regimes (vertical dashed lines).

Thus, positive and negative chirps ($\partial_\xi k_\beta > 0$ and $\partial_\xi k_\beta < 0$) exhibit qualitatively different behaviors, but both strongly mitigate the hosing instability (compared to the case with no chirp). In these cases, using the standard scaling Eq. (5)—which does not take into account this mitigation—can lead to an overestimation of the instability by an order of magnitude, or more. Qualitatively, this is because a betatron chirp causes the different slices of the bunch to progressively dephase and disrupts their coherent contribution to the instability after a length $L_{\rm sat}$. Note that the scaling $L_{\rm sat} \propto |\partial_\xi k_\beta|^{-3/2}$ cannot be obtained from a coarse two-particle model [25].

We note that the qualitative behavior for $\partial_\xi k_\beta < 0$, whereby the amplitude of the oscillations initially increases but later decreases, is consistent with the behavior shown in Ref. [11], where the authors observed, in numerical simulations, that the deceleration of the tail of driver bunch (which induces $\partial_\xi k_\beta < 0$) in the blowout regime could cause a similar decrease in amplitude.

Quasilinear wakefield with optimal beam loading.—Let us now connect the simplified case of a linear betatron chirp [Eq. (3)] with the more generic case of the quasilinear wakefield [Eq. (2)]. Here we will consider the important case where $n_b(\xi)$ is constrained by optimal beam loading. In order to produce monoenergetic beams, it is indeed desirable to tailor the beam density so as to flatten the accelerating field. The accelerating force on a narrow witness electron beam ($k_p r_b \ll 1$) is given by [21]

$$\frac{F_z(\xi)}{mc\omega_p} = -\eta_{d\|}\cos[k_p(\xi_d - \xi)] - [1 - k_p r_b K_1(k_p r_b)] \times \int_\xi^0 \frac{n_b(\xi')}{n_p}\cos[k_p(\xi' - \xi)]k_p d\xi', \tag{8}$$

where $\eta_{d\|}$ is the amplitude of the longitudinal driven wakefield. For example, $\eta_{d\|} = [1 - k_p r_d K_1(k_p r_d)] \times (n_d/n_p) 2\sin(k_p \ell_d/2)$ for a flattop electron bunch driver, and $\eta_{d\|} = \sqrt{\pi/8} \times a_0^2(\omega_p\tau)e^{-(\omega_p\tau)^2/2}$ for a Gaussian laser pulse. In these conditions, it is well known [21] that optimal beam loading (i.e., uniform accelerating field) is obtained for a triangular-shaped witness bunch, with (in our notation)

$$n_b(\xi) = \frac{n_p \eta_{d\|}}{[1 - k_p r_b K_1(k_p r_b)]}[\sin(k_p\xi_d) - \cos(k_p\xi_d)k_p\xi]. \tag{9}$$

Inserting this expression into the equations for the accelerating force [Eq. (8)] and the betatron frequency [Eq. (2)] yields

$$F_z(\xi) = -\eta_{d\|} mc\omega_p \cos(k_p\xi_d), \tag{10}$$

$$k_\beta^2(\xi) = \frac{k_p^2}{2\gamma}\frac{\eta_{d\|}}{[1 - k_p r_b K_1(k_p r_b)]}[\sin(k_p\xi_d) - \cos(k_p\xi_d)k_p\xi] + \frac{k_p^2}{2\gamma}\eta_{d\perp}\left(1 - \frac{(\eta_{d\|}/\eta_{d\perp})}{[1 - k_p r_b K_1(k_p r_b)]}\right)\sin[k_p(\xi_d - \xi)]. \tag{11}$$

According to Eq. (11), in the case of optimal beam loading, the form of the head-to-tail variations of $k_\beta(\xi)$ depends on the ratio of the transverse and longitudinal driven wakefield $\eta_{d\|}/\eta_{d\perp}$, and thus on the shape of the driver. For instance, for $\eta_{d\|}/\eta_{d\perp} = 1 - k_p r_b K_1(k_p r_b)$ (which occurs, e.g., for a narrow bunch driver with a

radius r_d equal to that of the witness beam r_b), the second term in Eq. (11) vanishes, and so $k_\beta(\xi)^2$ is simply linear in ξ, with a slope proportional to $-\cos(k_p\xi_d)$. Note that, in the accelerating phase of the wakefield, $\cos(k_d\xi_d) < 0$, and thus this situation corresponds to the regime $\partial_\xi k_\beta > 0$. On the other hand, for $\eta_{d\parallel}/\eta_{d\perp} \gg 1 - k_p r_b K_1(k_p r_b)$ (which is usually the case for a Gaussian laser driver, or a wide bunch driver) the variations of $k_\beta(\xi)$ are more complicated, with $\partial_\xi k_\beta$ changing sign from head to tail.

In order to illustrate these two situations, we carried out particle-in-cell (PIC) simulations with (a) a bunch driver having a radius $r_d = 1.25 r_b$ [which corresponds to $\eta_{d\parallel}/\eta_{d\perp} \approx 1 - k_p r_b K_1(k_p r_b)$, and thus $\partial_\xi k_\beta > 0$] and (b) a laser driver having $k_p w = 2$ [which corresponds to $\eta_{d\parallel}/\eta_{d\perp} \gg 1 - k_p r_b K_1(k_p r_b)$, and thus $\partial_\xi k_\beta < 0$ in most of the bunch]. For simplicity, we disabled driver evolution in the simulations, and imposed a driver velocity $v_d = c$. (This is valid for acceleration distances shorter than the characteristic length scale of driver evolution, which is on the order of $\gamma_d r_d^2/\epsilon_d$ for a beam driver with a normalized emittance ϵ_d, and on the order of the dephasing length k_0^2/k_p^3 for a guided laser driver.) In both simulations (which used $n_p = 2 \times 10^{17}$ cm^{-3}), a witness beam with $\gamma = 200$ was initialized with a longitudinal density $n_b(\xi)$ given by Eq. (9) (i.e., optimal beam loading), and a transverse Kapchinskij-Vladimirskij distribution [26] with a radius $r_b = 3$ μm and which was matched to $k_\beta(\xi)$ as given by Eq. (11) (thereby ensuring that the transverse density profile remains close to flattop throughout the simulation). In order to seed the hosing instability, the witness bunch was shifted transversally by an initial uniform offset $x_c(\xi, 0) = 0.12$ μm. The simulations were performed with the spectral quasicylindrical code FBPIC [27] using the azimuthal modes $m = 0$ and $m = 1$. (This is sufficient because the fields of the unperturbed, symmetrical beam are entirely contained in the mode $m = 0$, and because the perturbations due to the small offset x_c create additional contributions in the modes $m > 0$ with a typical amplitude $(x_c/r_b)^m$ [6]. Thus, if x_c is small compared to r_b, the relevant physics can be captured by the leading order, i.e., the mode $m = 1$.) In the simulations, the cell size was $\Delta z = 0.17$ μm and $\Delta r = 0.06$ μm, the time step was chosen such that $c\Delta t = \Delta z$, and the background plasma was represented with 8 macroparticles per cell (which was sufficient to reach numerical convergence, as ascertained by separate tests featuring 32 macroparticles per cell).

The PIC simulation results are shown in the upper panels of Fig. 2. As expected from the analysis of Eq. (11), the betatron frequency k_β exhibits head-to-tail variations in both cases (top plots). This causes the instability to quickly saturate as a function of z in the PIC simulations (upper color maps, showing that the maximum centroid offset reaches only a limited value on the logarithmic color scale), in a way that is consistent with the numerical integration of the equation of hosing Eq. (1) with k_β given by Eq. (11) (middle color maps). Importantly, the level of the instability is much lower than it would have been in the case of a uniform k_β (lower color maps, reaching higher values on the logarithmic color scale). This can also be seen on the lineouts of the color maps at a fixed position ξ (bottom plots), which, again, show that the PIC simulations and Eq. (1) with Eq. (11) are in agreement regarding the

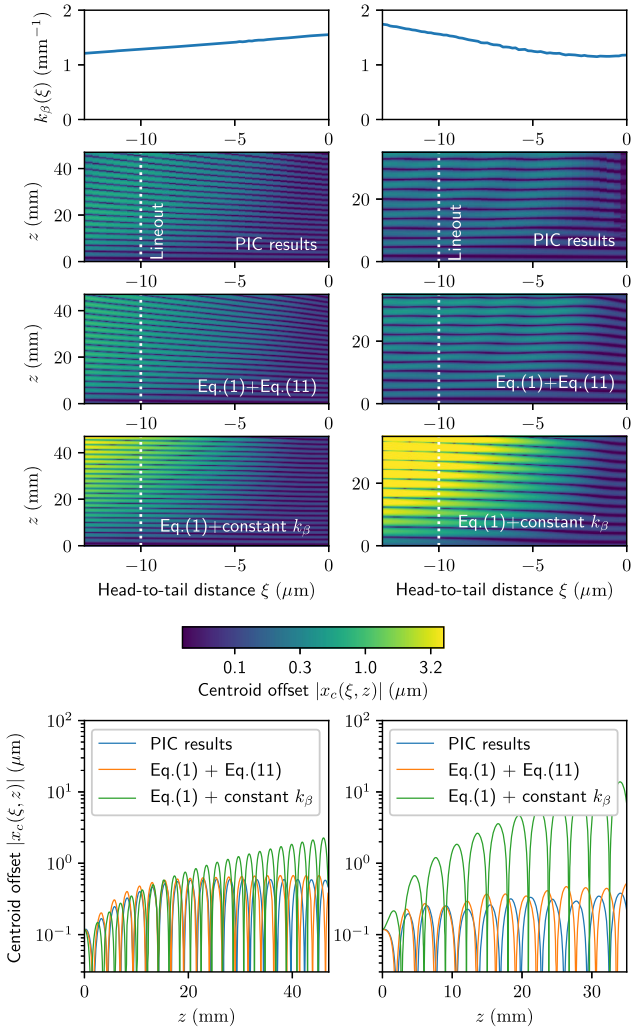

FIG. 2. Evolution of the centroid offset (log-scaled color map) as a function of the head-to-tail coordinate ξ and the propagation distance z, for [case (a); left-hand panels] a bunch driver with $r_d = 4$ μm, $\ell_d = 3$ μm, $\xi_d = 27$ μm, and $n_d = 0.7 n_p$, and [case (b); right-hand panels] a laser driver with $a_0 = 0.4$, $\tau = 20$ fs, $\xi_d = 26$ μm, $w = 24$ μm. The top plots show the head-to-tail variations of the betatron frequency k_β in both cases. The upper color maps show results from the PIC simulations, while the middle and lower color maps show results from the numerical integration of Eq. (1), with $k_\beta(\xi)$ either given by Eq. (11) (middle color maps) or considered uniform (lower color maps). The lower plots are lineouts of the color maps, at a fixed head-to-tail distance ($\xi = -10$ μm; indicated by a white dotted line on the color maps).

amplitude of the centroid oscillations [some differences occur because Eq. (1) neglects beam acceleration and the evolution of the transverse beam profile], and that this amplitude is lower than that predicted by Eq. (1) with a constant k_β. This confirms that, in the quasilinear regime, the hosing instability is less severe than suggested by the standard scalings [e.g., Eq. (5)] that assume a uniform k_β.

In conclusion, we showed that, in the quasilinear regime of plasma acceleration, the hosing instability is strongly mitigated, even for a monoenergetic bunch. This is due to the natural variations of the focusing forces across the bunch, and happens both for increasing and decreasing head-to-tail variations. In the case of optimal beam loading, the exact form of these head-to-tail variations is controlled by the shape of the driver.

This work was supported by the Director, Office of Science, Office of High Energy Physics, of the U.S. Department of Energy under Contract No. DE-AC0205CH11231. Simulations were performed on the Lawrencium computational cluster resource provided by the IT Division at the Lawrence Berkeley National Laboratory (supported by the Director, Office of Science, Office of Basic Energy Sciences, of the U.S. Department of Energy under Contract No. DE-AC02-05CH11231).

*rlehe@lbl.gov

[1] Y. Y. Lau, Phys. Rev. Lett. **63**, 1141 (1989).
[2] V. K. Neil, L. S. Hall, and R. K. Cooper, Part. Accel. **9**, 213 (1979).
[3] D. H. Whittum, J. Phys. A **30**, 8751 (1997).
[4] W. K. H. Panofsky and M. Bander, Rev. Sci. Instrum. **39**, 206 (1968).
[5] D. H. Whittum, W. M. Sharp, S. S. Yu, M. Lampe, and G. Joyce, Phys. Rev. Lett. **67**, 991 (1991).
[6] C. B. Schroeder, C. Benedetti, E. Esarey, F. J. Grüner, and W. P. Leemans, Phys. Rev. E **86**, 026402 (2012).
[7] A. W. Chao, B. Richter, and C.-Y. Yao, Nucl. Instrum. Methods **178**, 1 (1980).
[8] A. A. Geraci and D. H. Whittum, Phys. Plasmas **7**, 3431 (2000).
[9] E. S. Dodd, R. G. Hemker, C.-K. Huang, S. Wang, C. Ren, W. B. Mori, S. Lee, and T. Katsouleas, Phys. Rev. Lett. **88**, 125001 (2002).
[10] C. B. Schroeder, D. H. Whittum, and J. S. Wurtele, Phys. Rev. Lett. **82**, 1177 (1999).
[11] T. J. Mehrling, R. A. Fonseca, A. Martinez de la Ossa, and J. Vieira, Phys. Rev. Lett. **118**, 174801 (2017).
[12] C. Huang, W. Lu, M. Zhou, C. E. Clayton, C. Joshi, W. B. Mori, P. Muggli, S. Deng, E. Oz, T. Katsouleas, M. J. Hogan, I. Blumenfeld, F. J. Decker, R. Ischebeck, R. H. Iverson, N. A. Kirby, and D. Walz, Phys. Rev. Lett. **99**, 255001 (2007).
[13] V. Lebedev, A. Burov, and S. Nagaitsev, Rev. Accel. Sci. Techol. **09**, 187 (2016).
[14] P. Mora and J. Thomas M. Antonsen, Phys. Plasmas **4**, 217 (1997).
[15] J. B. Rosenzweig, B. Breizman, T. Katsouleas, and J. J. Su, Phys. Rev. A **44**, R6189 (1991).
[16] A. Pukhov and J. Meyer-ter Vehn, Appl. Phys. B **74**, 355 (2002).
[17] W. Lu, C. Huang, M. Zhou, W. B. Mori, and T. Katsouleas, Phys. Rev. Lett. **96**, 165002 (2006).
[18] M. Tzoufras, W. Lu, F. S. Tsung, C. Huang, W. B. Mori, T. Katsouleas, J. Vieira, R. A. Fonseca, and L. O. Silva, Phys. Rev. Lett. **101**, 145002 (2008).
[19] E. Esarey, C. B. Schroeder, and W. P. Leemans, Rev. Mod. Phys. **81**, 1229 (2009).
[20] V. E. Balakin, A. V. Novokhatsky, and V. P. Smirnov, in *Proceedings of the 12th International Conference on High-Energy Accelerators, HEACC 1983: Fermilab, Batavia, 1983* (Fermilab, Batavia, 1984), No. C830811, p. 119.
[21] T. C. Katsouleas, S. Wilks, P. Chen, J. M. Dawson, and J. J. Su, Part. Accel. **22**, 81 (1987).
[22] D. Chernin and A. Mondelli, Part. Accel. **24**, 177 (1989).
[23] See Supplemental Material at http://link.aps.org/supplemental/10.1103/PhysRevLett.119.244801 for a derivation of the analytical solutions in Eqs. (5)–(7).
[24] G. V. Stupakov, SLAC Report No. SLAC-AP-108, 1997.
[25] A. Chao, K. Mess, M. Tigner, and F. Zimmermann, *Handbook of Accelerator Physics and Engineering* (World Scientific Publishing Company, Singapore, 2013).
[26] S. M. Lund, T. Kikuchi, and R. C. Davidson, Phys. Rev. ST Accel. Beams **12**, 114801 (2009).
[27] R. Lehe, M. Kirchen, I. A. Andriyash, B. B. Godfrey, and J.-L. Vay, Comput. Phys. Commun. **203**, 66 (2016).